ACS OMEGA

http://pubs.acs.org/journal/acsodf

Article

Screening Physical Solvents for Methyl Mercaptan Absorption Using Quantum Chemical Calculation Coupled with Experiments

Pengju Liang, Sihui Duan, Qiang Ma, Liangliang Zhang, Guangwen Chu, and Bao-Chang Sun*

Cite This: *ACS Omega* 2023, 8, 11790−11800

Read Online

ACCESS | Metrics & More | Article Recommendations | Supporting Information

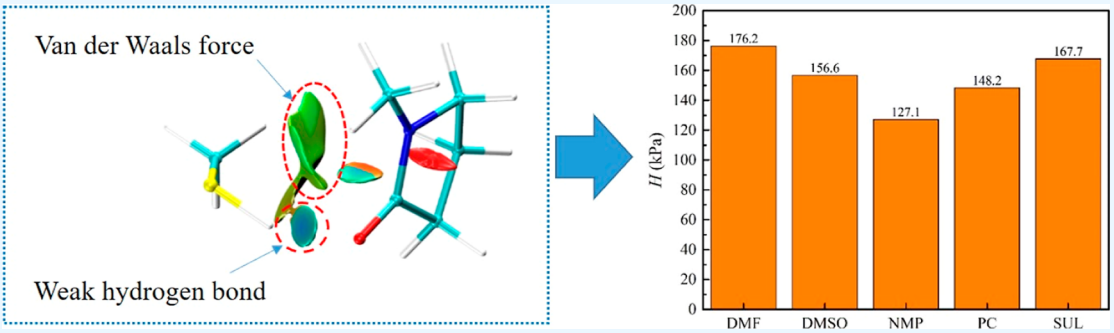

ABSTRACT: This work presents a screening method of physical solvents for methyl mercaptan (MeSH) absorption using quantum chemical calculations. The absorption solubility and thermodynamic behaviors of dimethyl sulfoxide (DMSO), sulfolane (SUL), propylene carbonate (PC), *N*,*N*-dimethylformamide (DMF), and 1-methyl-2-pyrrolidinone (NMP) for MeSH were calculated and analyzed using the COSMO-RS model, and the absorption mechanism was probed combining the quantum theory of atoms in molecules (QTAIM) and reduced density gradient (RDG). Results show that the absorption solubility of the five solvents for MeSH by COSMO-RS model calculations follow the order of NMP > PC > DMSO > SUL > DMF, and the van der Waals forces and hydrogen bond forces determine the absorption solubility of physical solvents for MeSH. In addition, the experimental results of MeSH Henry coefficients in the above five solvents follow the same order as the calculated results. However, the calculated Henry coefficients' value largely deviates from the experimental value; therefore, we believe that this calculation method is only available for qualitative screening. This work provided a feasible approach to screening high-performance physical solvents for MeSH removal.

1. INTRODUCTION

Natural gas usually contains H_2S and organosulfur, and the latter mainly includes carbonyl sulfide (COS), methyl mercaptan (MeSH), and thioether.[1,2] Before use, natural gas must be purified to remove sulfur compounds according to the corresponding standards. At present, alkanolamine absorption process is usually adopted in industries to simultaneously absorb H_2S and organosulfur.[2] Generally, alkanolamine solvents, including *N*-methyl diethanolamine (MDEA), monoethanolamine (MEA), and diethanolamine (DEA), have been reported for the simultaneous removal of H_2S and MeSH from natural gas.[3,4] These alkanolamine solvents present high removal capacity of H_2S, but a relatively low removal capacity of MeSH for the mass-transfer control of the MeSH absorption in alkanolamine solvents. Therefore, many researchers are committed to searching for a high-efficiency absorbent component to enhance MeSH absorption.

Physical solvents such as *N*-formylmorpholine (NFM), dimethylsulfoxide (DMSO), *N*-methylpyrrolidone (NMP), propylene carbonate (PC), polyethylene glycol dimethyl ethers, and sulfolane (SUL) with a higher efficiency for organosulfur absorption have been explored in refs 5−67. Shen et al.[8] calculated and prepared a hybrid UDS-2 solvent which contains SUL, cyclic amine, and MDEA for simultaneous absorption of H_2S, MeSH, and COS from sour natural gas, and results showed that SUL exhibited good physical solubility for MeSH and COS. Bedell and Miller[9] reported that physical solubility dominated the absorption of MeSH in aqueous amines, while the chemical solubility is diminished. Generally, some researchers have studied the absorption of MeSH in the gas stream using physical absorbers using quantitative calculations. However, a simple and fast approach to screen physical absorbers with a high absorption capacity for MeSH absorption is still desired.

Conductor-like screening model for real solvents (COSMO-RSs) as a novel, fast, and prior predictive method has been widely applied to predict the physical and thermodynamic

Received: September 24, 2022
Accepted: December 27, 2022
Published: March 24, 2023

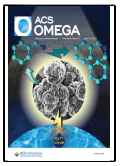

properties of liquid mixtures and solvents.[10,11] Palomar et al.[12] used the COSMO-RS model to investigate the absorptive capacity of ionic liquids (ILs) to CO_2 from power plant emissions, indicating that this model is an efficient and reliable method for the prediction of the absorption ability of ILs to CO_2. Sumon[13] calculated Henry's law constants of CO_2, CH_4, and N_2 in ILs by COSMO-RS at 283.15, 298.15, and 323.15 K. Qi et al.[14] employed COSMO-RS to predict infinite dilution activity coefficients of benzene and cyclohexane in different ILs to obtain high-efficient ILs for the separation of benzene and cyclohexane. Lei et al.[15] used the COSMO-RS model combined with the quantum chemistry calculation to screen ILs for absorption of benzene, toluene, and p-xylene. The COSMO-RS model has been proven a powerful theoretical method to guide the screening of ILs for absorption processes. Unfortunately, there are few reports about screening physical absorbers for absorption of MeSH using the COSMO-RS model. In addition, a deep understanding of the intermolecular interaction information and thermodynamic behavior between absorbents and MeSH is conducive to the screening process.

Quantum chemical calculations, including the quantum theory of atoms in molecule (QTAIM) topological analysis, noncovalent interaction (NCI)[16,17] analysis, and reduced density gradient analysis (RDG), have been generally applied to analyze intermolecular interaction forces,[18−20] which provides an effective method to obtain thermodynamic information of energetics, structures, and properties of atoms and molecules.[21−23] For example, Zhan et al.[24] screened solvents and analyzed the interaction of solvent−dimethyl disulfide (DMDS) for extractive distillation of DMDS from methyl *tert*-butyl ether compounds containing DMDS by RDG and QTAIM. Ren et al.[25] revealed the configuration feature and intermolecular interaction characteristics of asphaltene dimes using quantum chemical calculations. It was found that NCI and natural bond order (NBO) analysis identified the interactions promoting the formation of asphaltene dimers, and RDG revealed the type of interactions between the two asphaltene monomers in their dimers. Zhang[26] has screened physical solvents for the removal of MeSH by calculating binding energy between the solvent and organosulfur. These reviews show that quantum chemical calculation methods are helpful to deeply understand the mechanism of intermolecular interaction.

In this work, the Henry coefficients, excess enthalpies, σ-moments, and σ-profiles of MeSH in DMSO, SUL, PC, DMF, and NMP have been calculated by COSMO-RS to understand the thermodynamics behavior between them and screen out the highly efficient MeSH physical solvents. Furthermore, QTAIM and RDG have been calculated by Gaussian to explore the intermolecular interactions between physical solvents and MeSH. In addition, the MeSH absorption experiment was also carried out to validate the calculated MeSH absorption performance of different solvents. This work has provided a route to screen high-performance physical solvents for MeSH absorption.

2. COMPUTATIONAL METHODOLOGY AND EXPERIMENTS

2.1. COSMO-RS Calculation Process. The detailed theory of COSMO-RS can be found in the original work of Klamt.[11] The calculation process is divided into two steps. First, the molecular structure of all compounds (solvents and MeSH) is optimized in the Gaussian 09W package[27] at the B3LYP/6-31+G(d,p) computational level in the ideal gas. Then, vibrational frequency calculations are carried out on every optimized molecule to select the most stable conformer with minimum energy. Next, the ideal screening charges on the molecular surface for each species are calculated by the continuum solvation COSMO-RS model using the BVP86/TZVP/DGA1 level of theory, and the COSMO-RS file will be generated.[12] Second, the COSMO-RS file is used as an input file in the software COSMO-RS thermx17 (Version C30-1701 copyrighted by COSMO-RS logic Gmbh & Co.KG), which was developed to obtain the thermodynamic properties of solvent−MeSH systems. In this work, the parameter file BP-TZVP-C30-1401 was selected to calculate the thermodynamic properties of Henry coefficients, σ-moments, σ-profiles, and excess enthalpies.

σ-profile $[P^{xi}(\sigma)]$ is the probability of finding a mean screening charge density on a typical contact segment of a single molecule. The σ-profile $[P_S(\sigma)]$ is a sum of the σ-profiles of components x_i weighted with their mole fraction in the mixture of the whole system and can be calculated by

$$P_S(\sigma) = \frac{\sum_i x_i n^{x_i} P^{xi}(\sigma)}{\sum_i x_i n^{x_i}} \tag{1}$$

Intermolecular interactions are divided into three specific interactions: electrostatic-misfit energy (E_{MF}), hydrogen bonding energy (E_{HB}), and van der Waals energy (E_{vdW}),[10] which can be calculated by eqs 2−4, respectively

$$E_{MF} = a_{eff}\frac{\alpha}{2}(\sigma + \sigma') \tag{2}$$

$$E_{HB} = a_{eff} c_{HB} \min(0;\ \min(0;\ \sigma_{donor} + \sigma_{HB}) \times \max(0;\ \sigma_{acceptor} - \sigma_{HB})) \tag{3}$$

$$E_{VdW} = a_{eff}(\tau_{VdW} + \tau'_{VdW}) \tag{4}$$

Excess enthalpy H^E plays an indispensable role in the description of the nonideal thermodynamic behavior of the mixture systems. The COSMO-RS defines the excess enthalpy as the difference between the enthalpy of a solute molecule i in the mixture and that in the pure state

$$H_i^E(\text{interaction}) = H_{i,\text{mixture}}(\text{interaction}) - H_{i,\text{pure}}(\text{interaction}) \tag{5}$$

Here, the excess enthalpy of a certain molecule can be calculated by electrostatic misfit interaction (H^E_{MF}), van der Waals interaction (H^E_{VdW}), and hydrogen bonding interaction (H^E_{HB})[12]

$$H^E = H^E_{MF} + H^E_{VdW} + H^E_{HB} \tag{6}$$

A more detailed calculation process of COSMO-RS can be found in COSMO *therm* X User Guide and COSMO *therm* Reference Manual.

2.2. QTAIM and RDG Analyses. The Gaussian 09W with the approximate exchange−correlation energy function M06-2X employing the 6-311+G(d,p) basis set[27] was used to carry out quantum chemical calculation and get .fch or .fchk file and obtain wave function index. The Multiwfn program wave function analyzer software[28] was adopted to obtain the QTAIM and RDG. The parameters of electronic densities (ρ), energy densities, and Laplacian values ($\nabla^2\rho$) were

https://doi.org/10.1021/acsomega.2c06173
ACS Omega 2023, 8, 11790−11800

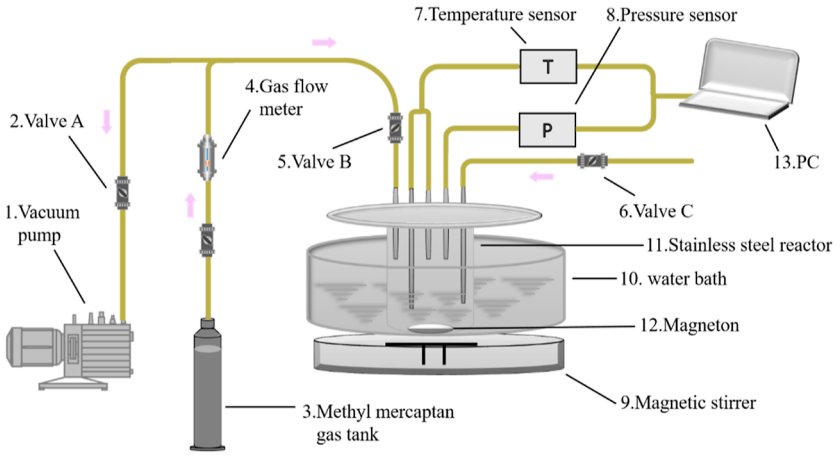

Figure 1. Schematic diagram of the experimental method.

obtained by the QTAIM calculation and can be used to qualitatively calculate the properties of the bond critical point (BCP) between the two molecules. Through the visual molecular dynamics (VMD) program, it was observed the strength and type of inter- or -intramolecular interactions visually.

2.3. Experiments. *2.3.1. Materials.* Dimethyl sulfoxide (99%, DMSO), SUL (99%), PC (98%), and *N*,*N*-dimethylformamide (99%) were purchased from Shanghai Aladdin Industrial Corporation. 1-Methyl-2-pyrrolidinone (98%, NMP) was obtained from the Beijing Chemical Works. Methyl mercaptan was purchased (99.99%, MeSH) from Beijing Zhaoge Gas Science and Technology Co., Ltd.

2.3.2. Experimental Process. The isochoric saturation method for the experimental process and the solubility was measured in a cylindrical stainless reactor with 170 mL, the liquid phase is stirred by a magnetic stirrer with magnon, and a diagram of the technological process is shown in Figure 1. The principle of the isochoric saturation method is like the pressure drop method, which is based on a known amount of gas contacting with the degassed solvents in a closed equilibrium cell at a constant temperature. The mass of solvents and the total cell volume are also known beforehand. During the dissolution process, the system pressure first decreases and then remains invariable to obtain the gas−liquid equilibrium, and then the Henry coefficients can be calculated after the balance.

The details of the experimental process are as follows: first, valve C was closed, valves A and B were opened, the reactor was vacuumized by a vacuum pump for 2 min and valves A and B were closed, and then the reactor system impermeability was examined until the value of the pressure sensor remained unchanged. Before every experiment, the same above approach needed to be carried out. Second, valve B was opened, the reactor vessel would be filled with MeSH gas, and the amount of MeSH could be regulated by gas flow meter 4. Third, 100 mL of organic solvent was injected into the reactor in each experiment via valve C. The reactor system temperature was controlled by water bath 10 and measured by temperature sensor 7. The solvent was stirred employing 9 magnetic stirrers to stir the liquid, then the vapor−liquid equilibrium obtained until the pressure in the reactor remained unchanged.

The solubility of MeSH in solvents expressed in the mole fraction can be calculated by

$$x_{MM} = \frac{n_{gas}^{liq}}{n_{gas}^{liq} + n_{liq}^{liq}} \tag{7}$$

where n_{liq}^{liq} is the number of solvents predetermined before the dissolution process, and n_{gas}^{liq} is the amount of gas dissolved into solvents calculated from the correlation of gas $P-V-T$.

Henry coefficients of gas absorbed are calculated using eqs 8−11. The initial moles of MeSH in the reactor vessel can be obtained by

$$n_{initial} = \frac{P_{initial}V_{initial}}{RT} \tag{8}$$

where initial pressure ($P_{initial}$) can be calculated by $P_{initial} = P_1 - P_0$; P_1 is the pressure of MeSH gas in the reactor; P_0 is vacuumed residual pressure of the reactor system; and $V_{initial}$ is the volume of the reactor.

The final moles of MeSH in the reactor vessel can be calculated by

$$n_{final} = \frac{P_{final}V_{final}}{RT} \tag{9}$$

where final pressure (P_{final}) can be calculated by $P_{final} = P_2 - P_0 - P_s$, P_2 is the final pressure of the reactor system, P_s is the saturated vapor pressure in the current temperature $V_{final} = V_{initial} - V_{liquid}$, and V_{liquid} is the volume of solvent in the reactor.

The solubility of MeSH was calculated in the solvent

$$x_i = \frac{n_g}{n_g + n_l - n_l^g} \tag{10}$$

where $n_g = n_{initial} - n_{final}$, n_l is the number of moles of solvent in a reactor.

The Henry coefficients were calculated as follows

$$H = \frac{P_{final}}{x_i} \tag{11}$$

3. RESULTS AND DISCUSSION

3.1. Henry Coefficients. In Figure 2, the predicted data of the COSMO-RS model for the physical solubility of MeSH in DMF, DMSO, NMP, PC, and SUL are shown. The calculated values of MeSH's Henry coefficients in five solvents were obtained following the order of NMP > PC > DMSO > SUL >

https://doi.org/10.1021/acsomega.2c06173
ACS Omega 2023, 8, 11790−11800

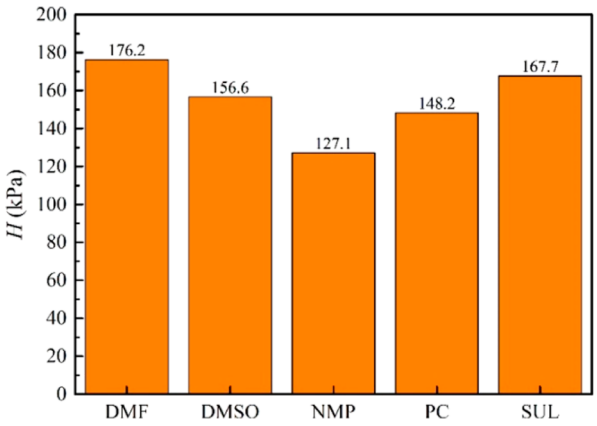

Figure 2. Henry coefficients of MeSH in different solvents (calculated value).

DMF, while the Henry coefficient in NMP is the lowest among the other solvents and thus has the maximum solubility for MeSH.

3.2. σ-Moment and σ-Profile Analyses. The σ-moments and molecular properties of solvents and MeSH are shown in Table.1. The σ-moment HB_{acc-3} is defined as the ability of the

Table 1. σ-Moments and Molecular Properties of Solvents and MeSH

component	HBacc-3	HBdon-3
MeSH	0.3254	0.0210
DMF	3.0538	0.003
DMSO	9.4314	0.0067
NMP	6.1866	0.0000
SUL	4.6662	0.0083
PC	1.4673	0.0000

HB acceptor (basicity), and the σ-moment HB_{don-3} is defined as the ability of the HB donor (acidity). Usually, a higher value of σ-moment means that it is easier to form HB. MeSH can act as both HB donor and HB acceptor, but its ability of HB donor with 0.0210 is weaker than that of a HB acceptor with 0.3254. MeSH also has difficultly in forming intermolecular HB resulting from its very low value of σ-moment. MeSH is usually an HB donor and forms HB with solvents which have a high HB_{don-3} value. On Table 1, the HB_{don-3} values of all DMSO, NMP, SUL, DMF, and PC are closer to zero compared to MeSH, which can act as an HB acceptor and generate HB with MeSH.

In the COSMO-RS model, the thermodynamic behaviors of mixtures related to σ-profiles are denoted by the molecular surface polarity distribution.[29,30] Based on molecular polarity, the whole σ region is divided into three parts: the σ in the range of $-0.0082 < \sigma\ (e/Å^2) < 0.0082$ presented at the middle position of the σ-profile curves is named the nonpolar region; the HB donor region is located at the range of $\sigma < -0.0082$ e/Å^2; and the HB acceptor region appears in the range of $\sigma > 0.0082$ e/Å^2. The component's σ-profile curves are shown in Figure 2.

As shown in Figure 3, MeSH had the strongest peak located at $-0.0084 < \sigma < 0$ which is caused by nonpolar H in C−H bonds and a slightly weaker peak located at $0 < \sigma < 0.0084$ resulting from the nonpolar C (corresponds with the green part of σ-surface for MeSH). This means that a strong

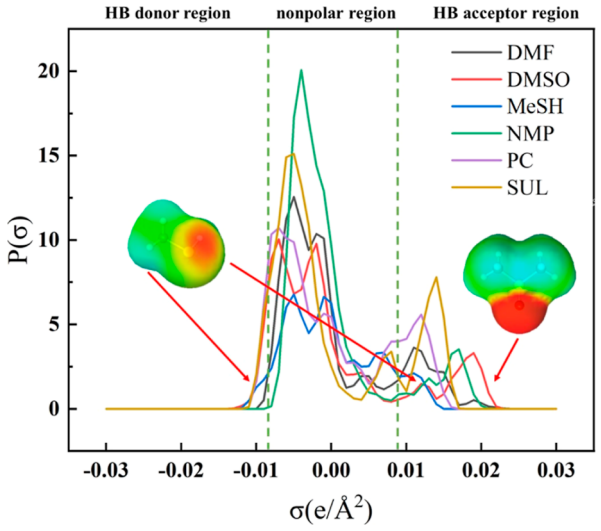

Figure 3. σ-Profile curves of MeSH, DMF, DMSO, NMP, SUL, PC, and the σ-surfaces of MeSH and DMSO.

nonpolar capacity and a strong attractive interaction with other components have nonpolar parts according to the like-dissolves-like principle. It is worth mentioning that MeSH had a weak peak in $\sigma = -0.012$ (corresponding with the light blue part of σ-surface) resulting from H in the S−H bond with a weak HB donor capacity. There was an HB acceptor region with a relatively strong peak lying in $0.01 < \sigma < 0.02$ (corresponding with the red part of σ-surface for MeSH), which is attributed to the strong polar character of S on the S−H group. For DMSO solvents, a peak in $\sigma = 0.018$ (dark red) was caused by sulfoxide oxygen (S═O), indicating that DMSO has an outstanding polar capacity and can form strong HB with MeSH. For other solvents, there were similar curves and trends to that of DMSO revealing that they had similar polar capacity properties. In addition, $P(\sigma)$ values and absolute σ values of had a positive interactive effect on polar capacity. The HB acceptor ability of five solvents followed the order of DMSO > NMP > DMF > SUL > PC. Therefore, from the analysis of the σ-profile of these solvents and MeSH, it can be deduced that strong interactions may be attributed to the polar capacity of solvents and MeSH. In addition, the formed HB between MeSH and solvents enhance solvents' solubility for MeSH.

3.3. Excess Enthalpy Analysis. The mixing process occurs both between the same component (solvent−solvents and MeSH−MeSH) and different components (MeSH−solvents). Therefore, the excess enthalpy is a useful thermodynamic property for understanding the difference in the strength of interactions between the different components via comparing with MeSH−solvents and solvent−solvents or MeSH−MeSH, which can provide insights into the behavior of the components in the solution. The excess enthalpy of MeSH in 5 solvents at 298.15 K is shown in Figure 4. The positive values of the excess enthalpy indicated that the MeSH absorption is an endothermic process, while the negative value means that it is an exothermic process. Endothermic behavior suggested that the attractive interaction between MeSH−MeSH or solvent−solvents is stronger than the mixtures of MeSH−solvents, exothermic behavior indicates that the attractive interactions between MeSH−solvents are stronger than MeSH−MeSH or solvent−solvents.

https://doi.org/10.1021/acsomega.2c06173
ACS Omega 2023, 8, 11790−11800

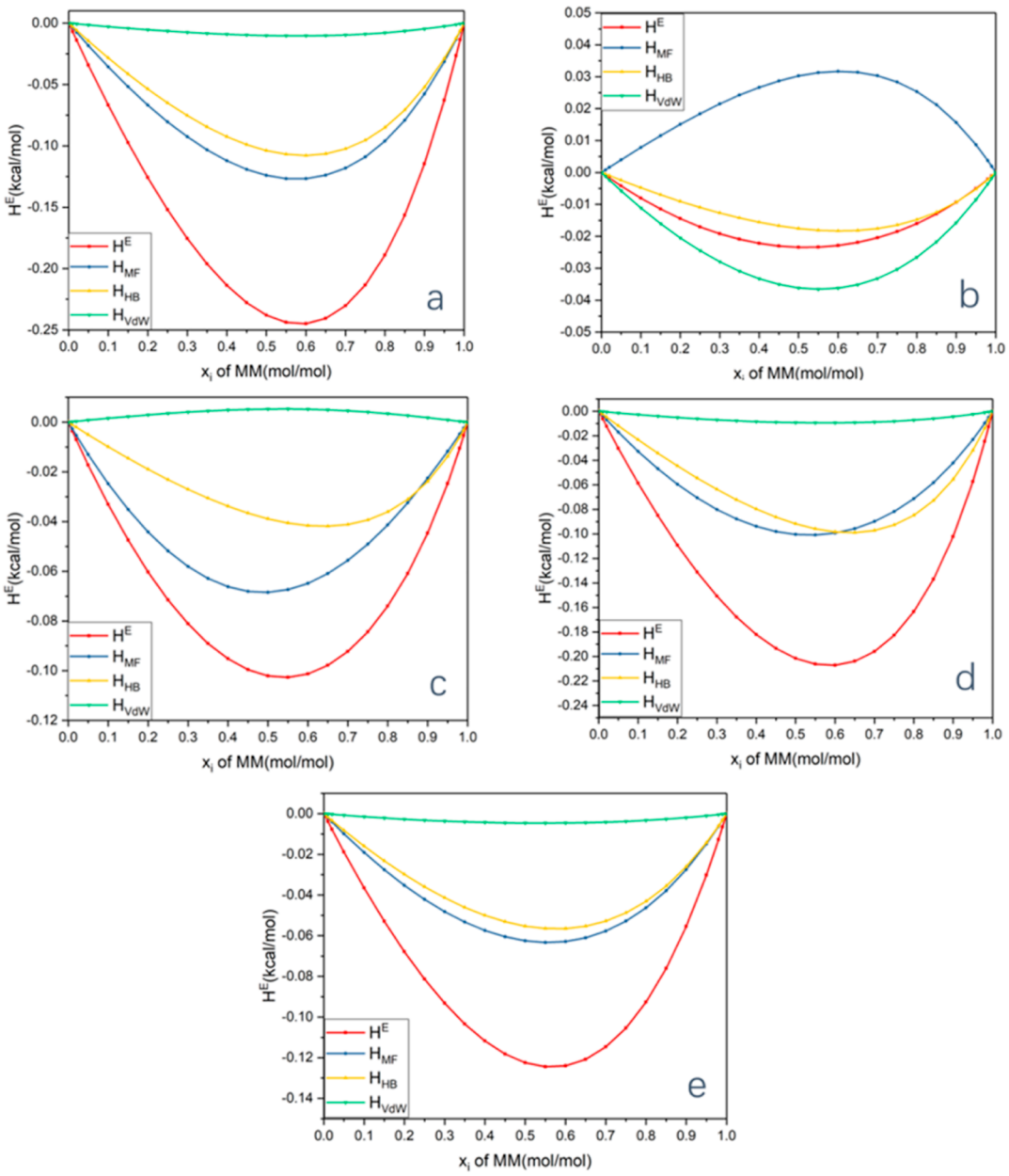

Figure 4. Contribution curves of hydrogen bond, van der Waals force, and misfit electrostatic force to excess enthalpy at 298.15 K (a) NMP−MeSH, (b) PC−MeSH, (c) SUL−MeSH, (d) DMSO−MeSH, and (e) DMF−MeSH.

Here, the excess enthalpy includes electrostatic-misfit interaction (H^E_{MF}), van der Waals interaction (H^E_{VdW}), and hydrogen bonding interaction (H^E_{HB}), which can be used to analyze the interactions between the components occurring in mixtures.[10] Hence, we calculated the energetics of 5 solvents at 298.15 K.

From Figure 4a, it can be obtained that: (i) the electrostatic-misfit interactions dominate the exothermic mixing process between NMP and MeSH because of the negative value for most (H^E_{MF}), and the contribution of hydrogen bonding interaction is slightly weaker than electrostatic-misfit interactions, which are favorable to intermolecular interactions between various components, leading to the higher solubility of MeSH in NMP relative to others. Here, the van der Waals interactions can be neglected as the value of (H^E_{VdW}) is almost zero. (ii) The addition of MeSH molar fraction decreased the electrostatic-misfit interaction between NMP and NMP, causing the negative value of (H^E_{MF}). (iii) The establishment of new hydrogen bonding between MeSH−NMP caused the MeSH−NMP mixing process to be exothermic. However, when x_i of MeSH > 0.6, the value of (H^E_{HB}) increases with the increase of x_i from 0.6 to 1. DMSO and DMF have similar trends with NMP.

For PC, the value of (H^E_{VdW}) was more negative than (H^E_{HB}) and the contribution of the van der Waals interaction played a key role during the three types of interactions in the mixing process. In addition, the value of (H^E_{MF}) was positive, which suggested that the electrostatic-misfit interaction caused the process to be slightly endothermic. However, the exothermicity caused by hydrogen bonding and van der Waals interactions was strong enough to overcome this slight endothermic process. Therefore, the whole mixing process was exothermic and the value of H^E was negative. For SUL, the values of (H^E_{MF}) and (H^E_{HB}) were negative, indicating this process was strongly

https://doi.org/10.1021/acsomega.2c06173
ACS Omega 2023, 8, 11790−11800

Table 2. BCP Analysis of Different Solvents and MeSH

		ρ (au×10^{-1})	H (au×10^{-3})	G (au×10^{-2})	V (au×10^{-2})	$\lvert V\rvert/G$	$\nabla^2\rho$ (au×10^{-1})	E_{HB} (kJ/mol)
DMF	28	0.0557	0.9464	0.4447	−0.3501	0.7872	0.2157	4.60
	23	0.1524	0.1013	1.1215	−1.1114	0.9910	0.4527	14.59
DMSO	19	0.1090	0.5897	0.8467	−0.7878	0.9304	0.3623	10.34
	32	0.0582	0.9669	0.3436	−0.2469	0.7186	0.1761	3.24
NMP	43	0.0732	1.0691	0.5795	−0.4726	0.8155	0.2746	6.20
	25	0.1429	0.4363	1.0977	−1.0541	0.9602	0.4565	13.84
	42	0.0779	1.0113	0.4897	−0.3885	0.7935	0.2363	5.10
SUL	24	0.1210	0.5468	0.9679	−0.9132	0.9435	0.4090	11.99
	25	0.1103	0.6148	0.8152	−0.7537	0.9246	0.3507	9.89
	41	0.0625	1.0450	0.3639	−0.2594	0.7128	0.1874	3.41
PC	48	0.0783	1.0333	0.6318	−0.5285	0.8365	0.2941	6.94
	42	0.0769	1.0217	0.6458	−0.5436	0.8418	0.2992	7.14
	23	0.0645	0.9931	0.3794	−0.2801	0.7382	0.1915	3.68
	28	0.0505	0.8083	0.2795	−0.1987	0.7108	0.1441	2.61

exothermic. The hydrogen-bonding interactions and electrostatic-misfit interactions influence each other during the mixing process, which leads to the high absorption performance of MeSH in SUL. The NMP had the lowest value of H^E at 0.6 x_i of MeSH.

In summary, excess enthalpy can be used to describe thermodynamic changes during the dissolution process. Solubilities of MeSH in solvents are related to the intermolecular interactions between solvents and MeSH, which are mainly affected by hydrogen bonding forces and van der Waals forces. To confirm this speculation, we conducted an intermolecular interaction analysis via QTAIM and RDG.

3.4. Intermolecular Interaction Analysis. *3.4.1. Quantum Theory of Atoms in Molecules.* QTAIM analysis has been utilized as a powerful tool for a detailed investigation of the nature of weak interactions in systems. QTAIM analysis uses electron density and its topology as the source of information for characterizing the types of interactions. According to the Bader's QTAIM theory, a BCP usually appears in the chemical bond path or between atom pairs, which have weak attractive interactions.

Further probing into the weak bonding interactions between solvents and MeSH was done by analyzing the values of topological descriptors, including density of all electrons (ρ), Laplacian of electron density ($\nabla^2\rho$), and the energy [H(r)] at the BCPs. The related parameters are listed in Table 2. Then, the type of interactions can be judged by $|V(r)|/G(r)$. When the ratio < 1, it means there is the closed interactions, when the ratio > 2, there is the share-type interactions. In addition, part of the covalent interactions and electrostatic interactions are observed in the range of $1 < |V(r)|/G(r) < 2$.

From Table 2, part of covalent and electrostatic interactions ($|V|/G$ = 1.0143) are found between the oxygen atom in the ring of NMP and the H atom in the S−H bonds of MeSH. The rest of the existing interactions with a closed-shell type (0.6500−1.0000) can be inferred.

In addition, it was found that when ρ was above 0.05 au, $\nabla^2\rho$ was positive, suggesting that there exists weak intermolecular interactions between solvent molecules and MeSH. Specifically, according to Koch and Popelier,[31] the HB interactions satisfied the criterion for the ρ parameters in the range of 0.002−0.035 au, with the corresponding Laplacian of electron density ($\nabla^2\rho$) values of 0.014−0.139 au. From Tabel 2, all parameters of ρ and $\nabla^2\rho$ agreed well with the above conditions. Hydrogen bonds are inferred between the O atoms of solvent molecules and H atoms of MeSH, as well as S atoms of MeSH and H atoms of solvent molecules. For a deeper understanding of the strength and position of hydrogen bonding at the BCP, the Espinosa−Molins−Lecomte formula ($E_{HB} = 0.5 \times V(r)$) has been used to calculate the E_{HB}, and BCP distribution obtained by QTAIM analysis is presented in Figure 5.

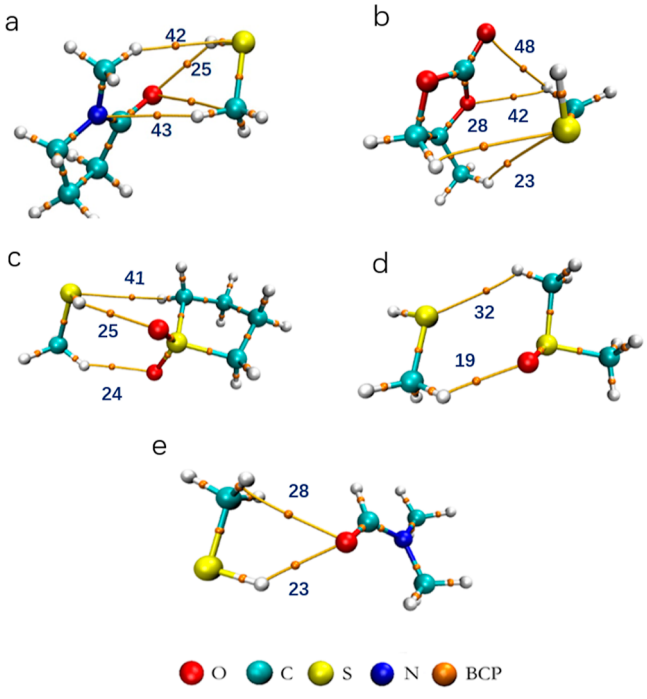

Figure 5. BCP distribution AIM analysis (a) NMP−MeSH, (b) PC−MeSH, (c) SUL−MeSH, (d) DMSO−MeSH, and (e) DMF−MeSH.

From Figure 5, every HB interaction has been shown, numbered, and expressed in the orange ball. In addition, two atoms connected by the orange line indicated an HB attractive interaction between these atoms. For DMSO, there are 2 HBs between DMSO and MeSH, which exist in S═O···H−C (19) and C−H···S−C (32). According to the E_{HB} value, the strength of HBs decreased following an order of 19 > 32.

According to the judgment of the interaction type, these HBs between solvents and MeSH meet the standard of weak

https://doi.org/10.1021/acsomega.2c06173
ACS Omega 2023, 8, 11790−11800

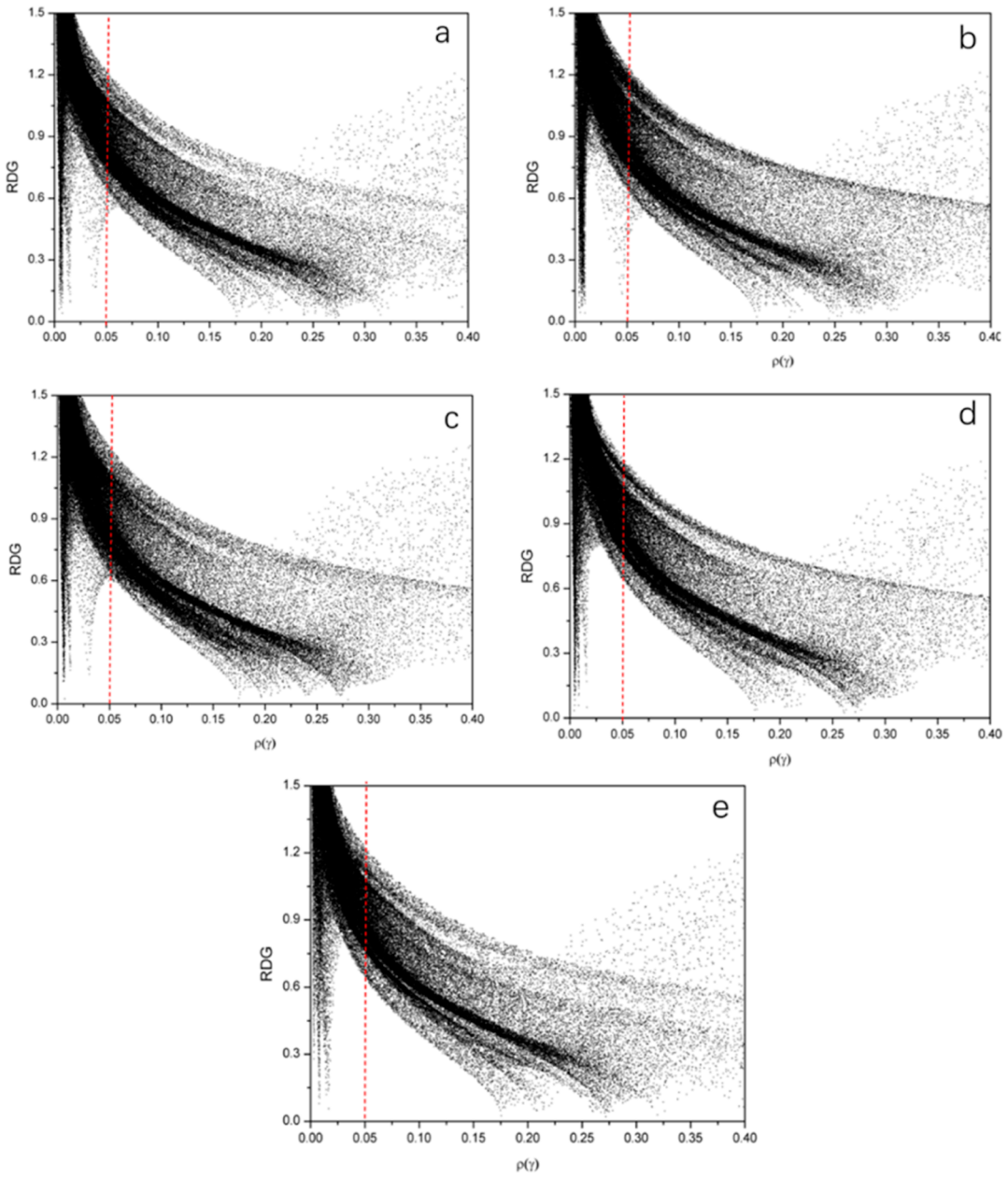

Figure 6. RDG-ρ(r) scatter diagram of solvent−MeSH system (a) NMP−MeSH, (b) PC−MeSH, (c) SUL−MeSH, (d) DMSO−MeSH, and (e) DMF−MeSH.

hydrogen bond, and it is weaker than traditional hydrogen bonds. On the other hand, the strength of HBs in S═O···H−S and C═O···H−S were all stronger than C−H···S−C, and the values of E_{HB} are all above 10 kJ/mol. It is worth noting that PC···MeSH almost had no strong HB because of the low value of E_{HB}, indicating that the solubility of MeSH in PC may not be affected by HB interactions, which agrees with the analysis of COSMO−RS.

3.4.2. Reduced Density Gradient. To gain greater insights into the weak interactions of solvent−MeSH mixtures, a reduced density gradient (RDG) analysis was performed. The relationships between RDG and ρ can be used to determine whether there exists a weak interaction.[18] Several spikes appeared when $\rho < 0.05$ and the corresponding RDG values are close to zero, proving the existence of weak interactions in the mixture. Specifically, when $\rho < 0.05$, there exists the noncovalent interaction in the mixture; when $\rho > 0.05$, there exists the covalent interaction in the mixture. Figure 6 shows the scatter maps of RDG versus ρ for DMSO−MeSH, PC−MeSH, DMF−MeSH, NMP−MeSH, and SUL−MeSH. In Figure 6, several spikes are found in the low-density ($\rho < 0.05$) and low RDG area, indicating that the weak interactions existed in all these mixtures.

To distinguish the interaction type, the relationship between the sign $(\lambda_2)\rho$ and RDG has been discussed, which serves as an effective tool to distinguish and visualize weak interactions: stabilized (HB), destabilized (steric repulsion), and delocalized weak forces (van der Waal). Therefore, by plotting RDG versus sign $(\lambda_2)\rho$, noncovalent interaction regions could be identified by analyzing spikes in Figure 7.

Figure 7 shows the relationship between the sign $(\lambda_2)\rho$ and RDG for different mixtures. To distinguish the type of weak

https://doi.org/10.1021/acsomega.2c06173
ACS Omega 2023, 8, 11790−11800

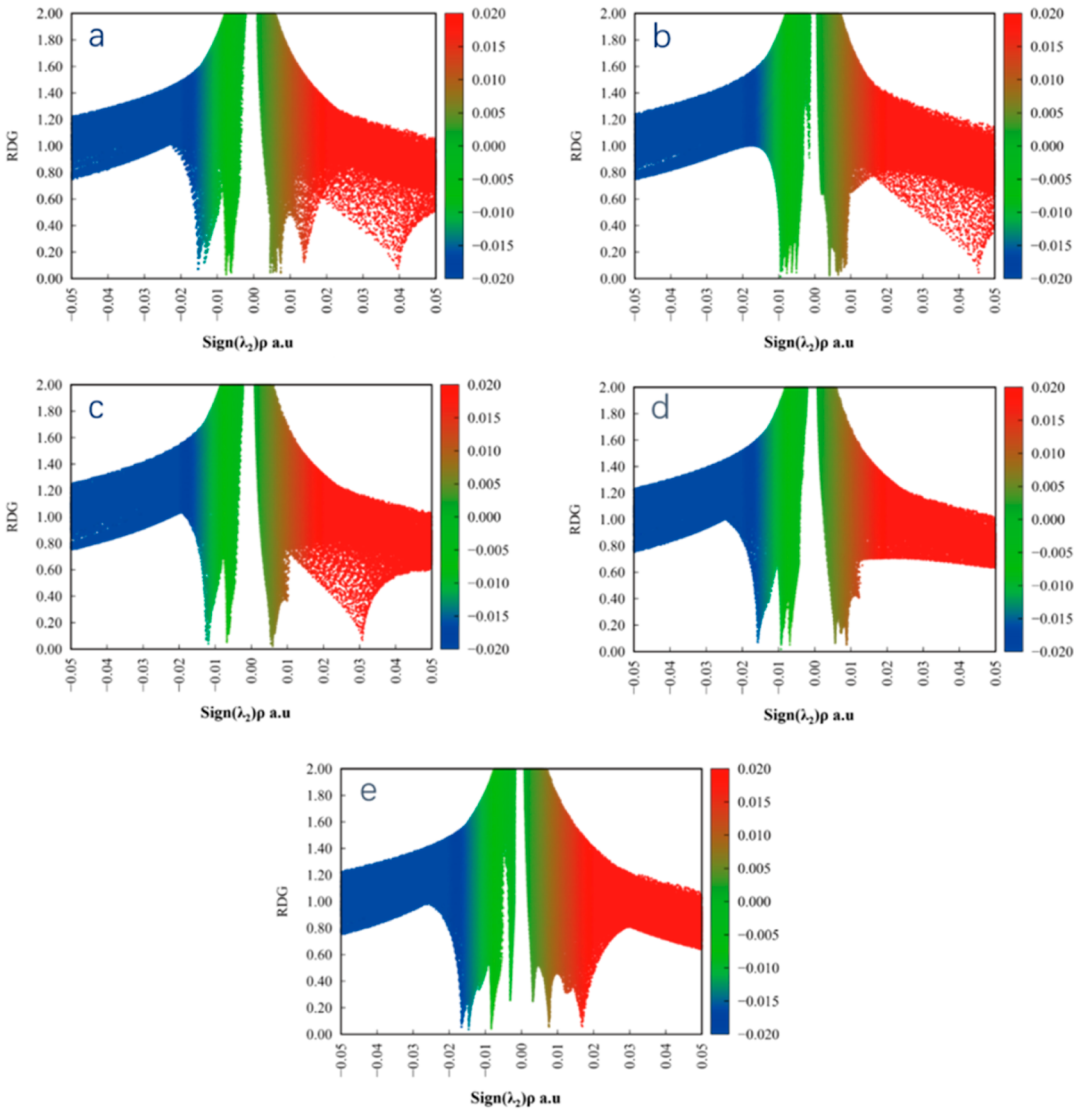

Figure 7. Fill color scatter diagram showing the plot of sign $(\lambda_2)\rho$ vs RDG for (a) NMP−MeSH, (b) PC−MeSH, (c) SUL−MeSH, (d) DMSO−MeSH, and (e) DMF−MeSH.

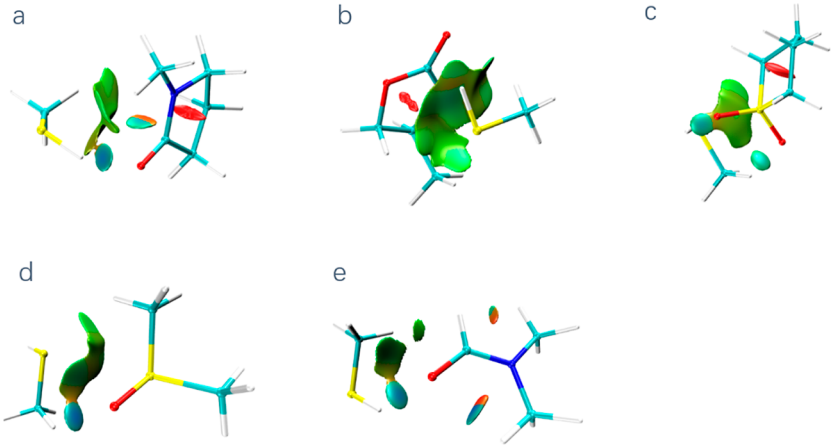

Figure 8. RDG equipotential surface coloring chart (a) NMP−MeSH, (b) PC−MeSH, (c) SUL−MeSH, (d) DMSO−MeSH, and (e) DMF−MeSH.

interactions, the following criteria can be referenced:[28] (i) spikes have appeared in the region of sign $(\lambda_2)\rho < 0$, indicating that the mixtures have attractive interactions, and corresponding spikes can be observed in the region of sign $(\lambda_2)\rho > 0$, suggesting the presence of dispersion interactions. (ii) The van der Waals region with spikes in the sign $(\lambda_2)\rho$ range of −0.005

https://doi.org/10.1021/acsomega.2c06173
ACS Omega 2023, 8, 11790−11800

to 0.005 indicates the existence of van der Waals forces in these mixtures. (iii) The stronger attractive interactions of HB appear in the region of sign $(\lambda_2)\rho < -0.01$ and spikes appear at sign $(\lambda_2)\rho > 0.01$ suggesting that the strong repulsive force (steric effect) exists in these mixtures. The strength of interaction can be reflected by the absolute value of sign $(\lambda_2)\rho$, and a larger absolute value means a stronger interaction.

According to the above criterion, NMP−MeSH, PC−MeSH, SUL−MeSH, DMSO−MeSH, and DMF−MeSH all have spikes in the region of sign $(\lambda_2)\rho < 0$, indicating they all had attractive interactions. For PC−MeSH, most spikes were distributed in the region of $-0.01 >$ sign $(\lambda_2)\rho > 0$, showing that there were no stronger attractive interactions between PC and MeSH. When sign $(\lambda_2)\rho > 0.04$, an obvious spike suggested the existence of a strong steric effect. The other three mixtures, all have spikes in < -0.01 and have a similar absolute value of sign $(\lambda_2)\rho$, indicating that they had the almost same strength of the attractive interactions. These were consistent with QTAIM results.

In addition, to visually observe the strength and position of those noncovalent interactions, the low-gradient (RDG = 0.5) isosurfaces were colored according to the corresponding values of effective density and displayed in Figure 8. The surfaces were colored on a blue-green-red scale with blue indicating strong attractive interactions (HB), green demonstrating weak interactions (such as van der Waals interactions), and red representing steric interactions.

The surfaces of PC−MeSH are composed of green and light blue, which meant there are no strong attraction interactions and the presence of van der Waals interactions, the red part of the surfaces indicated steric interactions among the ring structure of PC. This conclusion was consistent with that from the previous QTAIM and RDG analyses. For other MeSH−solvent mixtures, they had a distinct dark blue surface, suggesting that strong attraction interactions such as hydrogen bonding exist between solvents and MeSH. In addition, the vdW interaction and HB interaction were the important factors between the used solvents and MeSH through the gradient isosurfaces, and the hydrogen bonding force between MeSH and the used solvents promoted the dissolution process, which was consistent with COSMO−RS analysis.

In Figure 9, the experimental data for the physical solubility of MeSH in solvents at difficult temperatures are shown. The physical solubility trends of MeSH increased with the increases in temperatures for five sorts of solvents. The Henry coefficient of NMP was consistently lower than other solvents across the temperature range. This may be due to a higher degree of van der Waals force interactions between MeSH and NMP. However, Henry coefficients increased slightly with the temperature for the NMP solvent. The results also indicated that the solubility of MeSH in NMP is 2 times approximately higher than DMF. The linear relationship of 5 solvents' Henry coefficients versus temperatures was plotted at a range of 298.15 K $< T <$ 318.15 K, which are determined to be approximately 1.00 with regression values of $R^2 = 0.99$. For MeSH, the physical solubilities of the 5 solvents followed the order of NMP > PC > DMSO > SUL > DMF. These Henry coefficient changed trends were consistent with the calculated results by the COSMO−RS model, which indicated the method is fit for screening physical solvents of MeSH absorption from natural gas.

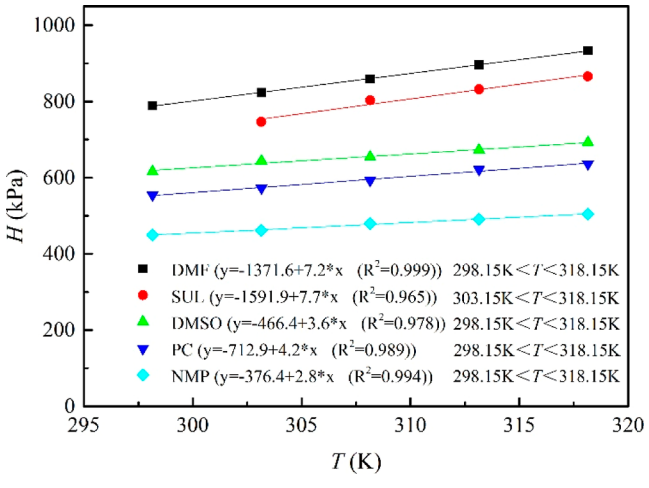

Figure 9. Henry coefficient of MeSH in solvents.

4. CONCLUSIONS

In this work, a method of combining the COSMO-RS analyses, quantum chemical calculations, and absorption desulfurization experiments was applied to screen the physical absorbents for the MeSH desulfurization sweetening process. From COSMO-RS analysis, five physical absorbents for absorbing MeSH have been screened. The result of σ-moments and σ-profiles and excess enthalpy of thermodynamic behavior analysis indicated that the van der Waals forces and hydrogen bond determine the absorption capacity of MeSH in physical absorbents. For QTAIM, theoretical analysis based on the values of ρ and $\nabla^2\rho$ and RDG analysis indicated that these weak interactions are composed of weak hydrogen bond and hydrogen bond and van der Waals interactions of intermolecular, which can reflect the solubilities of MeSH in solvents. The calculated sequence of solubilities for MeSH was NMP > PC > DMSO > SUL > DMF, which was consistent with the experimental results. This work proved that both calculation methods of COSMO-RS analysis and quantum chemical calculation can help us to screen out high-performance physical solvents for MeSH absorption quickly.

■ ASSOCIATED CONTENT

Supporting Information

The Supporting Information is available free of charge at https://pubs.acs.org/doi/10.1021/acsomega.2c06173.

Sigma profiles of NMP, PC, DMSO, SUL, DMF, and MeSH (XLSX)

■ AUTHOR INFORMATION

Corresponding Author

Bao-Chang Sun − *State Key Laboratory of Organic−Inorganic Composites, Beijing University of Chemical Technology, Beijing 100029, PR China; Research Center of the Ministry of Education for High Gravity Engineering and Technology, Beijing University of Chemical Technology, Beijing 100029, PR China;* orcid.org/0000-0002-3435-1250; Email: sunbc@mail.buct.edu.cn

Authors

Pengju Liang − *State Key Laboratory of Organic−Inorganic Composites, Beijing University of Chemical Technology, Beijing 100029, PR China; Research Center of the Ministry*

https://doi.org/10.1021/acsomega.2c06173
ACS Omega 2023, 8, 11790−11800

of Education for High Gravity Engineering and Technology, Beijing University of Chemical Technology, Beijing 100029, PR China

Sihui Duan − *State Key Laboratory of Organic−Inorganic Composites, Beijing University of Chemical Technology, Beijing 100029, PR China; Research Center of the Ministry of Education for High Gravity Engineering and Technology, Beijing University of Chemical Technology, Beijing 100029, PR China*

Qiang Ma − *Daqing Oilfield Kaipu Chemical Co., Ltd, Daqing 163414, P. R. China*

Liangliang Zhang − *State Key Laboratory of Organic−Inorganic Composites, Beijing University of Chemical Technology, Beijing 100029, PR China; Research Center of the Ministry of Education for High Gravity Engineering and Technology, Beijing University of Chemical Technology, Beijing 100029, PR China;* orcid.org/0000-0002-6812-6860

Guangwen Chu − *State Key Laboratory of Organic−Inorganic Composites, Beijing University of Chemical Technology, Beijing 100029, PR China; Research Center of the Ministry of Education for High Gravity Engineering and Technology, Beijing University of Chemical Technology, Beijing 100029, PR China;* orcid.org/0000-0002-3047-7024

Complete contact information is available at: https://pubs.acs.org/10.1021/acsomega.2c06173

Notes

The authors declare no competing financial interest.

■ ACKNOWLEDGMENTS

This work was supported by the National Natural Science Foundation of China (nos. 21878009, U1607114, and 21725601).

■ REFERENCES

(1) Rivera-Tinoco, R.; Bouallou, C. Reaction Kinetics of Carbonyl Sulfide (COS) with Diethanolamine in Methanolic Solutions. *Ind. Eng. Chem. Res.* **2013**, *47*, 7375−7380.

(2) Bedell, S. A.; Miller, M. Aqueous Amines as Reactive Solvents for Mercaptan Removal. *Ind. Eng. Chem. Res.* **2007**, *46*, 3729−3733.

(3) Rahman, M. A.; Maddox, R. N.; Mains, G. J. Reactions of Carbonyl Sulfide and Methyl Mercaptan with Ethanolamines. *Ind. Eng. Chem. Res.* **1989**, *28*, 470−475.

(4) Okonkwo, C. N.; Lee, J. J.; De Vylder, A. D.; Chiang, Y.; Thybaut, J. W.; Jones, C. W. Selective removal of hydrogen sulfide from simulated biogas streams using sterically hindered amine adsorbents. *Chem. Eng. J.* **2020**, *379*, 122349.

(5) Jamali, S. H.; Ramdin, M.; Becker, T. M.; Torres-Knoop, A.; Dubbeldam, D.; Buijs, W.; Vlugt, T. J. H. Solubility of sulfur compounds in commercial physical solvents and an ionic liquid from Monte Carlo simulations. *Fluid Phase Equilib.* **2017**, *433*, 50−55.

(6) Arthur, L.; KohlRichard, B.; Nielsen *Gas Purification*, 5th ed.; Gulf Professional Publishing. 1997; pp 1187−1237.

(7) Zhang, F.; Shen, B. X.; Sun, H.; Liu, J. C.; Shang, J. F. Simultaneous Removal of H_2S and Organosulfur Compounds from Liquefied Petroleum Gas Using Formulated Solvents: Solubility Parameter Investigation and Industrial Test. *China. Pet. Process. Pe.* **2015**, *17*, 75−81.

(8) Zhang, F.; Shen, B. X.; Sun, H.; Liu, J. C.; Liu, L. Rational Formulation Design and Commercial Application of a New Hybrid Solvent for Selectively Removing H_2S and Organosulfurs from Sour Natural Gas. *Energy Fuels* **2016**, *30*, 12−19.

(9) Bedell, S. A.; Miller, M. Aqueous Amines as Reactive Solvents for Mercaptan Removal. *Ind. Eng. Chem. Res.* **2007**, *46*, 3729−3733.

(10) Lei, Z. G.; Chen, B. H.; Li, C. Y. COSMO-RS modeling on the extraction of stimulant drugs from urine sample by the double actions of supercritical carbon dioxide and ionic liquid. *Chem. Eng. Sci.* **2007**, *62*, 3940−3950.

(11) Klamt, A. Conductor-like Screening Model for Real Solvents: A New Approach to the Quantitative Calculation of Solvation Phenomena. *J. Phys. Chem.* **1995**, *99*, 2224−2235.

(12) Palomar, J.; Gonzalez-Miquel, M.; Polo, A.; Rodriguez, F. Understanding the Physical Absorption of CO_2 in Ionic Liquids Using the COSMO-RS Method. *Ind. Eng. Chem. Res.* **2011**, *50*, 3452−3463.

(13) Sumon, K. Z.; Henni, A. Ionic liquids for CO2 capture using COSMO-RS Effect of structure, properties and molecular interactions on solubility and selectivity. *Fluid Phase Equilib.* **2011**, *310*, 39−55.

(14) Lyu, Z. X.; Zhou, T.; Chen, L. F.; Ye, Y. M.; Sundmacher, K.; Qi, Z. W. Simulation based ionic liquid screening for benzene-cyclohexane extractive separation. *Chem. Eng. Sci.* **2014**, *115*, 186−194.

(15) Yu, G. Q.; Dai, C. N.; Gao, H.; Zhu, R. S.; Du, X. X.; Lei, Z. G. Capturing Condensable Gases with Ionic Liquids. *Ind. Eng. Chem. Res.* **2018**, *57*, 12202−12214.

(16) Lefebvre, C.; Rubez, G.; Khartabil, H.; Boisson, J. C.; Contreras-García, C.; Hénon, E. Accurately extracting the signature of intermolecular interactions present in the NCI plot of the reduced density gradient versus electron density. *Phys. Chem. Chem. Phys.* **2017**, *19*, 17928−17936.

(17) Johnson, E. R.; Keinan, S.; Mori-Sánchez, P.; Contreras-García, J.; Cohen, A. J.; Yang, W. Y. Revealing Noncovalent Interactions. *J. Am. Chem. Soc.* **2010**, *132*, 6498−6506.

(18) Zhao, Y. S.; Pan, P. G.; Kang, X. J.; Tu, W. H.; Gao, H. S.; Zhang, X. P. Gas separation by ionic liquids: A theoretical study. *Chem. Eng. Sci.* **2018**, *189*, 43−55.

(19) Bendjemai, M.; Bouafia, H.; Sahli, B.; Dorbane, A.; Uğur, Ş.; Uğur, G.; Mokrane, S. Insight into the role of weak interactions on optoelectronic properties of $LiGaTe_2$ -chalcopyrite under pressure effect: DFT-D3, NCI and QTAIM investigations. *Phys. B* **2020**, *599*, 412463.

(20) Meng, C. C.; Zhang, S. Z.; Chen, Q. B.; Li, X. X.; Liu, H. L. Influence of Host-Guest Interaction between Chiral Selectors and Probes on the Enantioseparation Properties of Graphene Oxide Membranes. *ACS Appl. Mater. Interfaces* **2020**, *12*, 10893−10901.

(21) Liu, Y. Z.; Yu, T.; Lai, W. P.; Ma, Y. D.; Ge, Z. X.; Yang, F. L.; Zhou, P. P.; Zhang, Y. H.; Xie, K. F. Noncovalent functionalization of graphene through physisorption of 1,1-diamino-2,2-dinitroethene: Impacts of and cooperativity between hydrogen bond and $\pi\cdots\pi$ interaction. *J. Phys. Chem. Solids* **2021**, *148*, 109736.

(22) Bhattacharyya, S.; Bhattacherjee, A.; Shirhatti, P. R.; Wategaonkar, S. J. O-H···S Hydrogen Bonds Conform to the Acid-Base Formalism. *J. Phys. Chem. A* **2013**, *117*, 8238−8250.

(23) Zhang, Y. H.; Gao, H. R.; Wang, M. X.; Zhao, L.; Gao, J. S.; Xu, C. M. Research on the Effect of the Solvent Structure and Group on Separation of 1-Hexene, Benzene, and Thiophene. *Energy Fuels* **2019**, *33*, 5162−5172.

(24) Zhan, G. X.; Shen, B. X.; Sun, H.; Chen, X. Extractive Distillation Approach to the Removal of Dimethyl Disulfide from Methyl Tert-Butyl Ether: Combined Computational Solvent Screening and Experimental Process Investigation. *Ind. Eng. Chem. Res.* **2018**, *57*, 3348−3358.

(25) Wang, H. J.; Xu, H. Y.; Jia, W. H.; Liu, J.; Ren, S. L. Revealing the Intermolecular Interactions of Asphaltene Dimers by Quantum Chemical Calculations. *Energy Fuels* **2017**, *31*, 2488−2495.

(26) Sun, D. X.; Zhao, Y. L.; Cao, Y. J.; Liu, M. Q.; Zhang, Y. X.; Zhao, L.; Zhang, Y. H.; Gao, J. S.; Xu, C. M.; Hao, T. Z.; et al. Investigation on the Interaction Mechanism of the Solvent Extraction for Mercaptan Removal from Liquefied Petroleum Gas. *Energy Fuels* **2020**, *34*, 4788−4798.

(27) Frisch, M. J.; Trucks, G. W.; Schlegel, H. B.; Scuseria, G. E.; Robb, M. A.; Cheeseman, J. R.; Scalmani, G.; Barone, V.; Mennucci,

B.; Petersson, G. A.; et al. *Gaussian 09*, Revision E.01.; Gaussian, Inc.: Wallingford CT, 2013.
(28) Contreras-García, J.; Johnson, E. R.; Keinan, S. Program for Plotting Non-covalent Interaction Regions. *J. Chem. Theory Comput.* **2011**, *7*, 625−632.
(29) Lu, T.; Chen, F. W. Multiwfn: a Multifunctional Wavefunction Analyzer. *J. Comput. Chem.* **2012**, *33*, 580−592.
(30) Klamt, A.; Eckert, F. COSMO-RS: a novel and efficient method for the a priori prediction of thermophysical data of liquids. *Fluid Phase Equilib.* **2000**, *172*, 43−72.
(31) Koch, U.; Popelier, P. L. A. Characterization of C-H-O Hydrogen Bonds on the basis of the Charge Density. *J. Phys. Chem.* **1995**, *99*, 9747−9754.

https://doi.org/10.1021/acsomega.2c06173
ACS Omega 2023, 8, 11790−11800